

The synergistic effect of the multiple parameters of vibro-impact nonlinear energy sink

Petro Lizunov, Olga Pogorelova, Tetiana Postnikova*

Scientific Research Institute of Structural Mechanics, Kyiv National University of Construction and Architecture, 03680 Kyiv, Ukraine

* Corresponding author: Tetiana Postnikova, posttan@ukr.net

ARTICLE INFO

Received: 28 July 2023

Accepted: 4 September 2023

Available online: 12 September 2023

doi: 10.59400/jam.v1i3.199

Copyright © 2023 Author(s).

Journal of AppliedMath is published by Academic Publishing Pte. Ltd. This article is licensed under the Creative Commons Attribution License (CC BY 4.0). <https://creativecommons.org/licenses/by/4.0/>

ABSTRACT: This article studies the dynamics and efficiency of a vibro-impact damper (single-sided vibro-impact nonlinear energy sink—SSVI NES) depending on the exciting force parameters. The damper is coupled with a linear oscillator—the primary structure. It is shown that the damper is quite effective in a wide range of the exciting force amplitude and in the range of its frequency, which are higher than the resonant frequency; damper efficiency in these regions is fairly stable. The dynamics of the vibro-impact system “primary structure—SSVI NES” is rich and complex, which, however, does not impair the damper efficiency. In complex oscillatory regimes, the damper makes bilateral impacts: it hits both an obstacle and directly against the primary structure, which actually turns a single-sided NES into a double-sided one. The optimization procedure and the choice of optimal damper parameters play a very important role in damper design. Optimizing multiple damper parameters instead of three shows a synergistic effect and provides better results.

KEYWORDS: vibro-impact; damper; primary structure; obstacle; efficiency; complex dynamics

1. Introduction

For many years, scientists and engineers look for ways to mitigate unwanted vibrations in many areas of technology. Various vibration control devices have been developed. They can be classified into passive, active and hybrid control systems. Passive control devices have become widespread due to their reduced complexity and independence from a constant power source. One of the most popular types of passive control devices are tuned mass dampers (TMDs)^[1,2]. In their simplest form, TMDs consist of a supplemental mass that is coupled linearly to a structure. They have been implemented in a good number of buildings including very tall structures.

Over the past two decades, new devices for passive vibration control have been actively discussed in the world scientific literature. This device is nonlinear energy sink—NES^[3]. Its main difference from TMD is that the NES is attached to a primary structure via essentially nonlinear coupling. Its mass is much less than the primary structure mass, it is recommended to have a mass of 1% of the main body mass. Due to its nonlinearity, it can absorb part of the main body energy, that is, mitigate its vibrations. It is believed that these devices can be used, in particular, to mitigate vibrations in high-rise structures caused by impulse loads, wind and even seismic. In a modern review^[4], the authors write, “It will be very attractive research topic for thorough analysis, analytical numerical and experimental, that is expected to

reveal more information and findings to the underlying nonlinear dynamical behavior and facilitate the implementation of NESs in real-life structures and applications in the future.” Numerous analytical, numerical and experimental studies of NESs are described in the world scientific literature. Comprehensive reviews of modern researches on NESs^[4–8], monographs^[9], dissertations^[10–12] and articles^[13–16] are presented. Experimental studies are carried out both on small laboratory setups^[17,18] and on large - sized equipment, close to the real design, such as an 11 - ton 9 - floor frame structure^[19]. In this base structure, six NESs were installed, two of them were vibro - impact ones.

Many various types of NESs with different nonlinearity kinds are considered. One of them is a vibro - impact NES—single-sided SSVI NES and double-sided DSVI NES. Their main difference is a restoring force with a discontinuity, which is the result of an impact^[10]. The vibro - impact NES—VI NES, is believed one of the most effective.

The dynamic behavior of the “primary structure—NES” system and the damper efficiency, like any strongly nonlinear system, depend both on the system parameters and on the excitation parameters. Therefore, the problem of choosing the optimal damper parameters comes to the fore^[13,19–22]. In a review^[4], the authors write, “Most works use contour plots to find the optimal performance when comparing only two NES parameters. These neglects taking into consideration the potential synergistic effects of the multiple NES parameters induced due to the high nonlinearity in the system.” In this work, we compared the dynamic behavior and efficiency of the SSVI NES with the optimization of three and seven damper parameters and showed a synergistic effect from such consideration.

The literature discusses the important problem of the frequency response function of a main structure without and with a damper. In the study of Li^[11], the author writes that adding a damper reduces the resonance peak by producing two other small peaks located on either side of the resonance frequency. In the study of Javidialesaadi and Wierschem^[20], the authors also show two peaks of frequency response curve at optimized damper parameters.

One of the most important damper parameters to be optimized, along with its mass, stiffness, clearance, is the Newtonian restitution coefficient, which takes part in the description of an instantaneous impact. Its influence on the VI NES dynamics and efficiency is studied in many articles^[11,13,23,24]. In few works^[25,26], another way of impact simulation is considered; a finite contact duration model of a VI NES is proposed in the study of Feudo et al.^[26]. In the study of Theurich and Krac^[27], the authors note that the use of a Hertzian-type contact model eliminates “the need to resort to an empirical coefficient of restitution”.

After examining the impact simulation problem^[28,29], we have chosen a “more realistic model of impact process”^[30], namely impact simulation using Hertz’s contact law in accordance with his quasi-static contact theory^[31]. This law application makes it possible to take into account the mechanical characteristics of all colliding surfaces in more detail and accurately. In this article, we have shown that a softer impact provides better results. One of the latest articles devoted to comparing the effect of soft and hard impacts in a vibro - impact system is the study of Costa et al.^[32].

In this paper, we continue the study of the SSVI NES dynamic behavior, started in our previous papers^[33–35]. When studying the synergistic effect of the multiple parameters of VI NES, we observed complex oscillatory modes with rich dynamics that arise in the system for certain parameters set. In particular, we have observed and shown transient chaos, an interesting regime that has been studied in a number of works^[36,37].

The goals of this paper are:

- show the SSVI NES efficiency with changing the exciting force parameters;
- show the rich complex dynamics of the vibro - impact system “primary structure—VI NES” and its influence on the damper efficiency;
- show the effect of the optimization procedure on the system dynamics and the damper efficiency, in particular, the synergistic effect of optimizing the set of parameters;
- show the double - sided damper impacts against both the primary structure and the obstacle;
- show the ranges of exciting force parameters in which VI NES is effective.

2. Mathematical model

We consider a mechanical two-mass 2 - DOF vibro - impact system, which consists of a primary structure coupled with a vibro - impact damper, which corresponds to the conceptual scheme of the SSVI NES^[10,35]. A primary structure is a linear oscillator with mass m_1 attached to a fixed wall by a linear elastic spring with a stiffness k_1 and a damper with a damping coefficient c_1 . A vibro - impact damper of much smaller mass m_2 is attached to a primary structure by a linear elastic spring with a stiffness k_2 and a damper with a damping coefficient c_2 . The vibro - impact system is excited by an external harmonic force $F(t)$. The vibro - impact damper, moving along the base without friction, hits an obstacle rigidly connected to the primary structure. These impacts cause a strong system nonlinearity, which should ensure the energy transfer from the primary structure and, consequently, reduce it. However, as it will be shown below, the damper also directly hits the primary structure, which enhances the system nonlinearity and helps the implementation of complex motion modes with bilateral impacts^[35]. The distance specifications are as follows: x_1, x_2 are the bodies coordinates; the zero mark of the x -axis is at the primary structure mass center in an equilibrium state when all springs are not deformed. D is the initial distance between the bodies, i.e., the length of the undeformed right spring. C is the distance to the right movable wall, which defines the clearance (**Figure 1**).

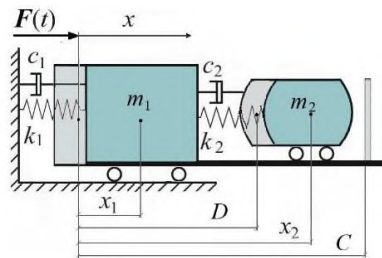


Figure 1. Calculation scheme of SSVI NES.

Primary structure parameters that are set in advance and cannot be changed, $m_1 = 1000$ kg, $k_1 = 3.95 \times 10^4$ N·m⁻¹, $c_1 = 452$ N·s·m⁻¹, $E_1 = 2.1 \times 10^{11}$ N·m⁻².

The motion equations for this system are as follows:

$$\begin{aligned} m_1 \ddot{x}_1 + c_1 \dot{x}_1 + k_1 x_1 - c_2 (\dot{x}_2 - \dot{x}_1) - k_2 (x_2 - x_1 - D) = \\ F(t) - H(z)F_{con}(z) + H(z_1)F_{con}(z_1) \\ m_2 \ddot{x}_2 + c_2 (\dot{x}_2 - \dot{x}_1) + k_2 (x_2 - x_1 - D) = \\ +H(z)F_{con}(z) - H(z_1)F_{con}(z_1) \end{aligned} \quad (1)$$

Exciting harmonic force $F(t) = P \cos(\omega t + \varphi_0)$. Its period $T = 2\pi/\omega$. The initial conditions are at $t = 0$, we have

$$x_1(0) = 0, x_2(0) = D, \dot{x}_1(0) = 0, \dot{x}_2(0) = 0, \varphi_0 = 0 \quad (2)$$

The terms $H(z)F_{con}(z)$ are associated with the impact rule. After examination of different methods of impact simulation^[28-30], we use Hertz's quasi - static contact theory^[31]. According to this theory, the impact has a finite duration and is modeled by a nonlinear force $F_{con}(z)$ acting only during the impact:

$$F_{con}(z) = K[z(t)]^{3/2} \quad (3)$$

where, z is the colliding bodies rapprochement upon impact.

The Heaviside step function $H(z) = \begin{cases} 1, & z \geq 0 \\ 0, & z < 0 \end{cases}$ ensures its activation upon impact. Then we have:

for the damper impacts directly on the primary structure for the damper impacts on an obstacle

$$K = \frac{4}{3} \frac{q}{(\delta_1 + \delta_2)\sqrt{A + B}} \quad K_1 = \frac{4}{3} \frac{q_1}{(\delta_3 + \delta_4)\sqrt{A_1 + B_1}}$$

$$\delta_1 = \frac{1 - \nu_1^2}{E_1\pi}, \delta_2 = \frac{1 - \nu_2^2}{E_2\pi} \quad \delta_3 = \frac{1 - \nu_3^2}{E_3\pi}, \delta_4 = \frac{1 - \nu_4^2}{E_4\pi} \quad (4)$$

These impacts occur when

$$x_1 \geq x_2, \text{ that is, } x_1 - x_2 \geq 0, z = x_1 - x_2 \quad x_2 \geq x_1 + C, \text{ that is, } x_2 - x_1 - C \geq 0, z_1 = x_2 - x_1 - C$$

where E_1, E_2, E_3, E_4 are Young's moduli of elasticity for fourth colliding surfaces; $\nu_1, \nu_2, \nu_3, \nu_4$ are Poisson's ratios; A, A_1, B, B_1, q, q_1 are constants characterizing the contact zones geometry. The damper surfaces, both left and right, are assumed to be spherical with large radii R and R_1 ; the contact surfaces of the primary structure and the obstacle are flat. Then $A = B = 1/2R, A_1 = B_1 = 1/2R_1$, we set $A = A_1 = B = B_1 = 0.5 \text{ m}^{-1}; q = q_1 = 0.319$ as in the collision of a plane and a sphere.

Taking into account the mechanical characteristics of the colliding surfaces makes it possible to analyze their influence on the system responses in more detail than more prevalent consideration of the Newtonian restitution coefficient^[35].

The total energy of the primary structure is calculated by the well - known formula:

$$E_{1total}(t) = E_{1kinetic}(t) + E_{1poten}(t) = \frac{m_1 \dot{x}_1(t)^2 + k_1 x_1(t)^2}{2} \quad (5)$$

3. Effect of an optimization procedure

An optimization procedure is recommended and often used in the investigations of NESs. The main goal of this optimization is to maximize the effective damping measure, which indicates the intensity of the efficient energy dissipation during the response to the external excitation; this damping is due to a strong nonlinearity of NES. So, the primary goal of the design - optimization process was to achieve a design that would be effective in attenuating the primary structure energy.

We will show how the choice of optimal values of many damper parameters instead of their small number affects the dynamics of a vibro-impact system consisting of a primary structure and NES coupled with it.

We carried out the optimization procedure in three stages using the `fmincon` and `fminsearch` solvers of the MATLAB platform. At the first stage, we employed it to select the optimal values of damper mass m_2 , stiffness k_2 and impact - surface clearance C of the NES physical system, given the preselected parameters of the primary structure. The oscillatory amplitude of the primary structure was chosen as the objective function for the optimization, since the minimum amplitude provides the minimum velocity and, consequently, the minimum energy. As result of optimization, two variants of the damper parameters were chosen. At the second stage, the optimal values of the Young's moduli of elasticity of

the colliding surfaces E_2 and E_4 were selected, which are introduced when simulating the impact according Equations (3) and (4) instead of the more familiar restitution coefficient. At last, at the third stage, we optimized the damping coefficient c_2 and damper initial distance from the primary structure D . So, the optimal values for 7 damper parameters were found.

There was a synergistic effect from the determination of 7 parameters compared with the determination of 3 parameters at the first stage of optimization. Let us show it.

After first stage of the optimization procedure, two significantly different results were chosen for further analysis:

$$\begin{aligned} m_2 &= 22.7 \text{ kg}, k_2 = 2481 \text{ N}\cdot\text{m}^{-1}, C = 0.0683 \text{ m}, \\ m_2 &= 37.9 \text{ kg}, k_2 = 414.6 \text{ N}\cdot\text{m}^{-1}, C = 0.0747 \text{ m}. \end{aligned}$$

Other parameters were not optimized in the first stage:

$$c_2 = 40.7 \text{ N}\cdot\text{s}\cdot\text{m}^{-1}, D = 0.050 \text{ m}, E_2 = 2.10 \times 10^{11} \text{ N}\cdot\text{m}^{-2}, E_4 = 2.10 \times 10^{11} \text{ N}\cdot\text{m}^{-2}, \nu_2 = \nu_4 = 0.3.$$

The vibro - impact damper, NES, coupled to the primary structure, provides the attenuation of its vibrations. The nonlinear damper transfers the energy from the primary structure and reduces it.

The decrease in the maximum total energy of the primary structure depending on the exciting force amplitude is shown in the **Figure 2a**. **Figure 2b** shows the total energy depending on time at $P = 800 \text{ N}$. The vibration mitigation occurs in a wide range of the exciting force amplitude at any amplitude. A heavier damper does the job better, its efficiency is higher. The damper efficiency is quite stable, despite the complex oscillatory regimes that occur with the changing in the exciting force amplitude. There are the periodic modes of different periodicity with a different impacts number per cycle both on the primary structure and on the obstacle; chaotic regimes and transient chaos also occur.

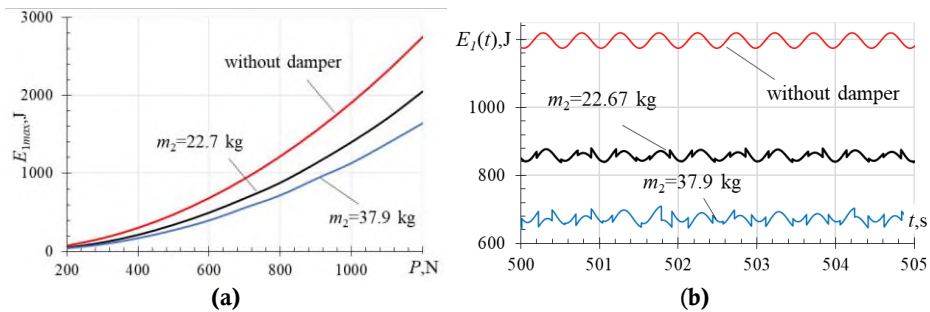


Figure 2. The decrease of the total energy of the primary structure coupled with SSVI NES with 3 optimized parameters when $\omega = 6.4 \text{ rad}\cdot\text{s}^{-1}$, **(a)** maximum total energy $E_{1\max}$ depending on the exciting force amplitude P ; **(b)** total energy $E_1(t)$ depending on time for $P = 800 \text{ N}$.

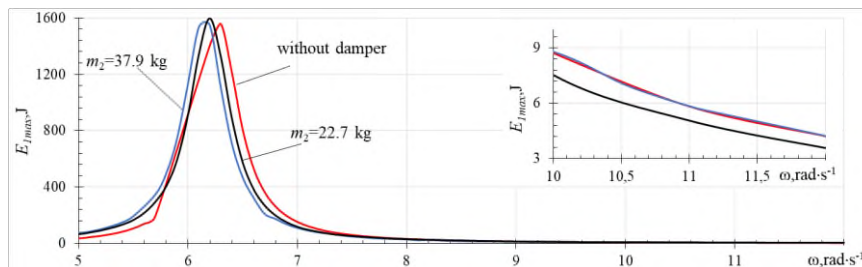


Figure 3. The decrease of the maximum total energy of the primary structure coupled with SSVI NES with 3 optimized parameters depending on the exciting force frequency when $P = 800 \text{ N}$.

Figure 3 shows the decrease in the primary structure energy in dependence on the exciting force frequency. First, note that vibration mitigation does not occur over the entire frequency range. The

resonant peak shifts to the left towards lower frequencies, but remains high, even slightly above the peak of the primary structure without damper, depicted by red curve. A heavier damper shows the higher efficiency. It is quite high in the most dangerous zone near the resonance, where the primary structure energy is large. In the frequency range where vibrations are mitigated, the damper efficiency is quite stable, despite the rich dynamics with complex oscillatory regimes.

Let's see what changes in the system dynamics provide the choice of 7 optimal damper parameters. Two significantly different optimization results were chosen for further analysis:

$$m_2 = 22.7 \text{ kg}, k_2 = 2481 \text{ N}\cdot\text{m}^{-1}, C = 0.0683 \text{ m}, c_2 = 41.4 \text{ N}\cdot\text{s}\cdot\text{m}^{-1}, D = 0.046 \text{ m}, E_2 = 2.26 \times 10^7 \text{ N}\cdot\text{m}^{-2}, E_4 = 2.18 \times 10^7 \text{ N}\cdot\text{m}^{-2}, m_2 = 37.9 \text{ kg}, k_2 = 414.6 \text{ N}\cdot\text{m}^{-1}, C = 0.0747 \text{ m}, c_2 = 27.9 \text{ N}\cdot\text{s}\cdot\text{m}^{-1}, D = 0.057 \text{ m}, E_2 = 2.21 \times 10^7 \text{ N}\cdot\text{m}^{-2}, E_4 = 2.05 \times 10^7 \text{ N}\cdot\text{m}^{-2}, \nu_2 = \nu_4 = 0.4.$$

A decrease by 4 orders of Young's moduli of elasticity E_2, E_4 shows that soft impacts of the damper both on the primary structure and on an obstacle are more preferable. The Young's moduli of colliding surfaces E_1, E_2 and E_3, E_4 are equal in the Equation (4), therefore, it does not matter which of them changes. Changing both moduli at the same time does not change the system response. Changing Poisson's ratios ν_2, ν_4 also does not change the system response. However, we chose $\nu_2 = \nu_4 = 0.4$, because these values correspond to materials with such low Young's moduli.

Figure 4a shows the decrease in the maximum total energy of the primary structure depending on the exciting force amplitude; **Figure 4b** depicts the total energy as a function of time at $P = 800 \text{ N}$. **Figure 5** shows the energy decrease in dependence on the exciting force frequency.

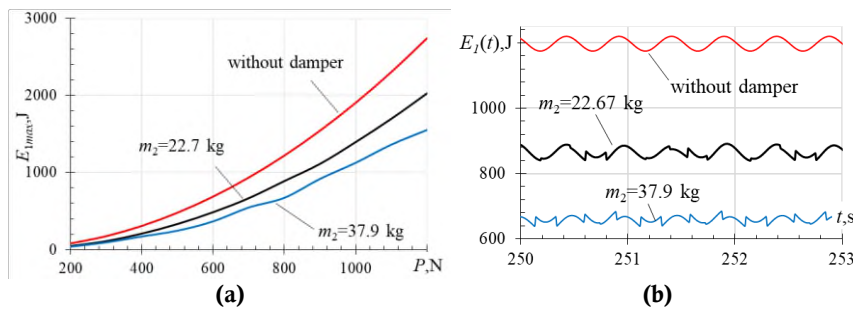


Figure 4. The decrease of the total energy of the primary structure coupled with SSVI NES with 7 optimized parameters when $\omega = 6.4 \text{ rad}\cdot\text{s}^{-1}$, **(a)** maximum energy E_{1max} depending on the exciting force amplitude P ; **(b)** total energy $E_1(t)$ depending on time for $P = 800 \text{ N}$.

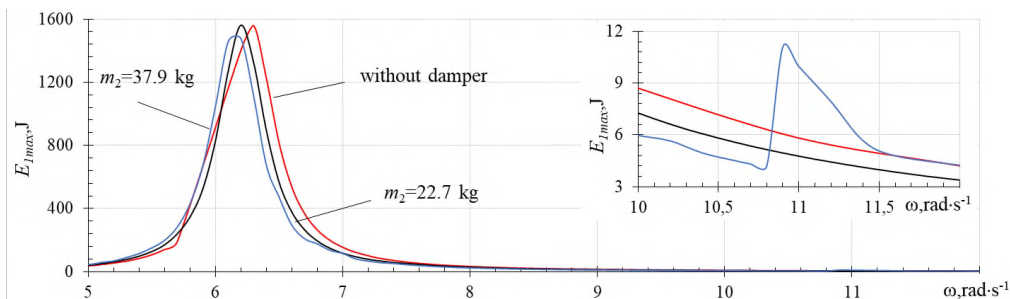


Figure 5. The decrease of the maximum total energy of the primary structure coupled with SSVI NES with 7 optimized parameters depending on the exciting force frequency when $P = 800 \text{ N}$.

Comparing **Figures 2** and **3** with **Figures 4** and **5** shows that the overall dynamic picture is the same. As in the previous case, the resonant peak shifts to the left towards lower frequencies and remains high. However, a second resonant peak appears at high frequencies (**Figure 5**). It is small, appears only for a

heavier damper. There is no energy attenuation in its region, but this is not so important, since the primary structure energy for these frequencies is small. This frequency response is similar to that of a detuned TMD^[10]. **Figure 5**, like **Figure 3** shows a decrease in the primary structure energy at sufficiently high frequencies above the resonance one. At low frequencies below resonant one energy attenuation does not occur. The resonant peak shifts to the left towards low frequencies, as in **Figure 3**. But unlike **Figure 3**, for a heavier damper it decreases somewhat. Perhaps other optimization procedures will allow us to find a different damper design that provides greater reduction in the resonant peak. This is a task for the future.

However, the main synergistic effect is manifested in a significant difference in the implemented motion regimes and a slight improvement in damper efficiency. These differences are clearly visible in **Tables 1 and 2**. The top records correspond to the responses of the system with 3 optimized damper parameters, bottom records—with 7 optimized parameters.

Table 1. Energy reduction depending on the value of the exciting force amplitude at $\omega = 6.4 \text{ rad}\cdot\text{s}^{-1}$.

P, N	200	500	700	800	900
$E_{1\max}$ wane in % at $m_2 = 22.7 \text{ kg}$	34.9	28.1	27.0	27.7	26.8
	39.1	30.3	28.6	27.1	28.0
Regime	2T, 0, 3; rare bursts	T, 1, 3; rare bursts	Alternation: T, 1, 2; 2T, 4, 6; rare bursts	T, 1, 2; chatter; rare bursts	Intermittency
	3T, 0, 3	T, 1, 2	T, 1, 2	4T, 8, 8	T, 2, 3
$E_{1\max}$ wane in % at $m_2 = 37.9 \text{ kg}$	46.2	42.6	40.1	41.0	39.8
	50.8	48.6	41.5	44.9	40.6
Regime	T, 1, 1; rare bursts	T, 2, 2; rare bursts	Chaotic	Chaotic	Chaotic
	(T, 1, 1)	Transient chaos; (T, 2, 2)	Chaotic	Transient chaos; (T, 2, 3)	Chaotic

Table 2. Energy reduction depending on the value of the exciting force frequency at $P = 800 \text{ N}$.

$\omega, \text{rad}\cdot\text{s}^{-1}$	6.2	6.3	6.4	6.5	6.7	7.0	7.5	10.0
$E_{1\max}$ wane in % at $m_2 = 22.7 \text{ kg}$	-13.8	14.7	26.6	28.9	26.2	23.2	15.0	13.6
	-11.1	15.2	27.1	30.5	27.9	24.2	13.5	16.4
Regime	Chaotic	Chaotic; intermittency	Chaotic; intermittency	Chaotic; intermittency	T,1,2	T,0,2	T, 0, 2; rare bursts	T, 0, 1
	Chaotic	Chaotic	4T, 8, 8	T, 1, 2	T, 1, 2	T, 1, 2	T, 0, 1	T, 0, 1
$E_{1\max}$ wane in % at $m_2 = 37.9 \text{ kg}$	-10.5	28.7	41.4	42.0	42.4	28.3	19.9	-1.1
	-5.1	28.7	44.9	42.0	43.0	25.3	26.9	31.2
Regime	Intermittency	Chaotic	Chaotic	Chaotic	T, 2, 2	Chaotic	T, 1, 1; rare bursts	T, 0, 0
	Transient chaos; T, 3, 3	Chaotic	Transient chaos; T, 2, 3	Chaotic	Transient chaos; T, 2, 2	Chaotic	T, 1, 1	T, 1, 1

Following the logic of the study Lamarque and Janin^[38], we use the notation nT, k, m , which defines the regime of periodicity nT (where T is the exciting force period) with k impacts between the damper and the primary structure and m impacts of the damper on an obstacle.

Table 2 emphasizes that a decrease of the primary structure energy occurs at sufficiently high exciting force frequencies. At lower frequencies, the energy increases, and we show this increase as a decrease with a minus sign. This frequency response demonstrates the limitations of VI NES.

Table 2 also shows that a rich complex dynamic is realized in a vibro-impact system consisting of a primary structure coupled to a NES. Indeed, in the study of Saeed et al.^[4], the authors note this phenomenon as one of the VI NES disadvantages, “One disadvantage of VI NESs is that coupling it with a primary structure leads to very complex nonlinear dynamics that is difficult to analyze analytically without making several simplifications.” It is important to emphasize that, despite such complex dynamics, the damper efficiency remains quite stable. This is due to the fact that the amplitudes and velocities of the heavy primary structure change little when complex motion modes arise. In this case, the impact contact forces change greatly.

Then **Table 2** shows the presence of direct impacts between the damper and the primary structure^[33–35]. This means that the single-sided VI NES practically works like a double-sided one, where the primary structure plays the role of a second obstacle. There are the modes with a different number of damper impacts per cycle, both on the primary structure and on the obstacle.

One of the significant changes in the optimization of 7 damper parameters is the absence of bursts in the implemented regimes. Both periodic and chaotic modes become smoother, without even rare bursts. During the burst, the primary structure energy rises sharply; the damper efficiency is reduced.

Let us look at a striking example of a complex regime in which two different periodic modes $T, 1, 2$ and $2T, 4, 6$ alternate and are accompanied by rare bursts (**Figure 6**). This complex regime is implemented in a system with 3 optimized damper parameters at $\omega = 6.4 \text{ rad}\cdot\text{s}^{-1}$, $P = 700 \text{ N}$, $m_2 = 22.7 \text{ kg}$, and it is that turns into a simple calm periodic $T, 1, 2$ regime in a system with 7 optimized damper parameters.

On **Figure 6a** one can clearly see sharp changes in the regime nature with the invariance of any parameters. The relative damper displacements $(x_2 - x_1)$ show one impact on the primary structure directly at $x_2 - x_1 = 0$ and two impacts on an obstacle per cycle T at $x_2 - x_1 = C = 0.0683 \text{ m}$ for $T, 1, 2$ regime and 4 impacts on the primary structure and 6 impacts on an obstacle per cycle $2T$ for $2T, 4, 6$ regime (**Figure 6b,c**). The graphs of impact contact forces confirm this statement: one “blue” force and two “green” forces per cycle for $T, 1, 2$ regime and 4 “blue” forces and 6 “green” forces per cycle $2T$ for $2T, 4, 6$ regime. The exciting force $F(t)$ is also shown in these figures; it is less contact forces by several orders of magnitude.

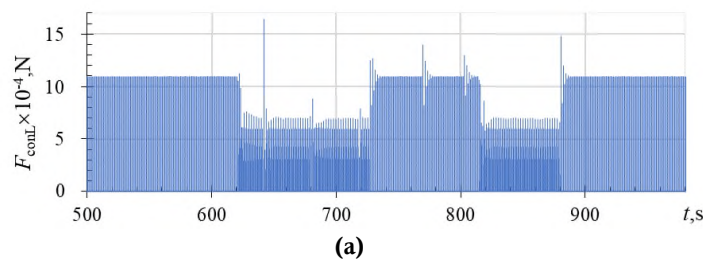


Figure 6. (Continued).

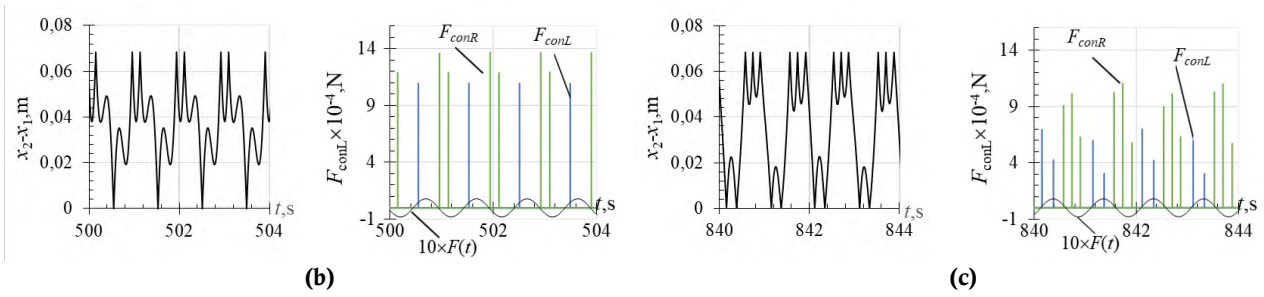


Figure 6. The motion picture in complex regime in which the modes $T, 1, 2$ and $2T, 4, 6$ alternate and are accompanied by rare bursts, **(a)** the contact forces during damper impacts on the primary structure; **(b)** and **(c)** the relative damper displacements and the contact forces during the damper impacts against the primary structure in blue and on an obstacle in green: **(b)** for $T, 1, 2$ regime; **(c)** for $2T, 4, 6$ regime.

4. Characteristics of the complex dynamic mode

Let us give as an example the characteristics of the regime implemented in the system with a damper of mass $m_2 = 37.9$ kg with 7 optimized parameters at $P = 800$ N, $\omega = 6.4$ rad·s⁻¹. In both tables it is called “transient chaos; $T, 2, 3$ ”. **Figure 7** shows the general picture of this movement. The displacements of primary structure are shown in black, the damper displacements are shown in gray in **Figure 7a**; the impact contact forces when the damper hits the primary structure are shown in blue in **Figure 7b**; the impact contact forces when the damper hits an obstacle are shown in green in **Figure 7c**. It is clearly seen how the chaotic motion is transformed into periodic one without any changes in any parameters. Changes in amplitudes are small, but in contact forces they are significant.

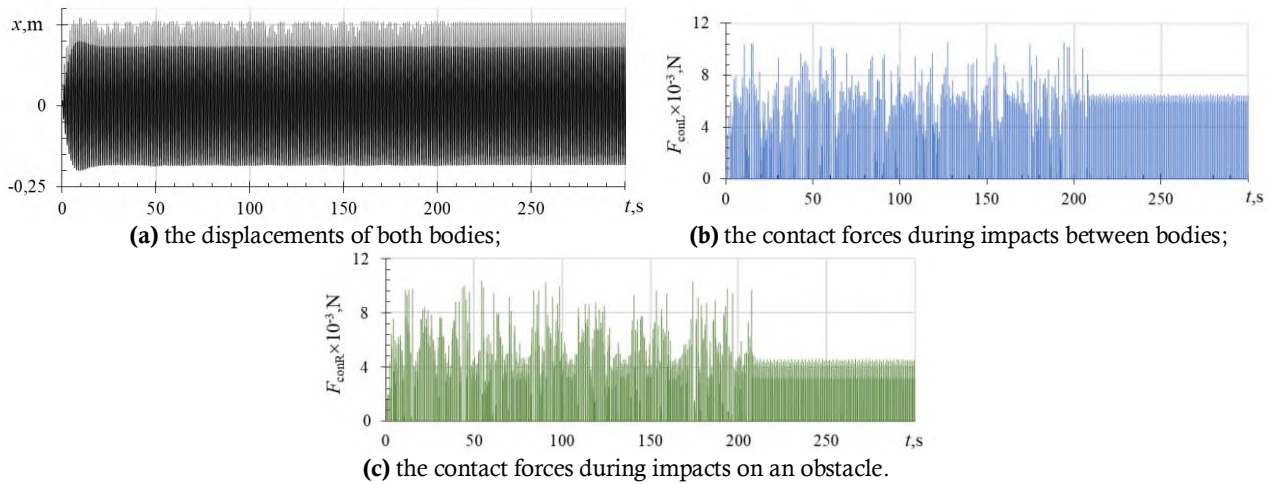


Figure 7. The general picture of transient chaos at $m_2 = 37.9$ kg with 7 optimized parameters at $P = 800$ N, $\omega = 6.4$ rad·s⁻¹.

Figure 8 shows the characteristics of both motion phases—chaotic on the left panel and periodic on the right. **Figures 8a** show the displacements of the damper and primary structure; they change little. The graphs of the relative damper displacements in **Figure 8b** show the damper impacts on the obstacle at $x_2 - x_1 = C = 0.075$ m and on the primary structure at $x_2 - x_1 = 0$; in the right figure we see 3 impacts on the obstacle and 2 hits on the primary structure per cycle in the periodic phase for $T, 2, 3$ regime. The same result is visible on the graphs of impact contact forces (**Figure 8c**): 3 “green” forces during impacts against the obstacle and 2 “blue” forces per cycle during impacts between bodies in the periodic phase. In this phase, the “blue” forces at impacts between bodies are greater the “green” forces at impacts on an

obstacle. In both phases, the impact forces are much greater than the exciting force, which is shown in brown in these graphs.

Figure 8d–g depict phase trajectories with Poincaré maps highlighted in red for the primary structure (**Figure 8d,f**) and the damper (**Figures 8e,g**). Their forms are typical for such modes: a ball of trajectories and a smear of the Poincaré map for the chaotic regime and a closed curve with one point of the Poincaré map for the periodic one. Finally, **Figure 8h,i** represent the total energy of the primary structure depending on time. **Figure 8i** also show its potential and kinetic energy. One can clearly see a significant reduction of the total energy due to the damper presence.

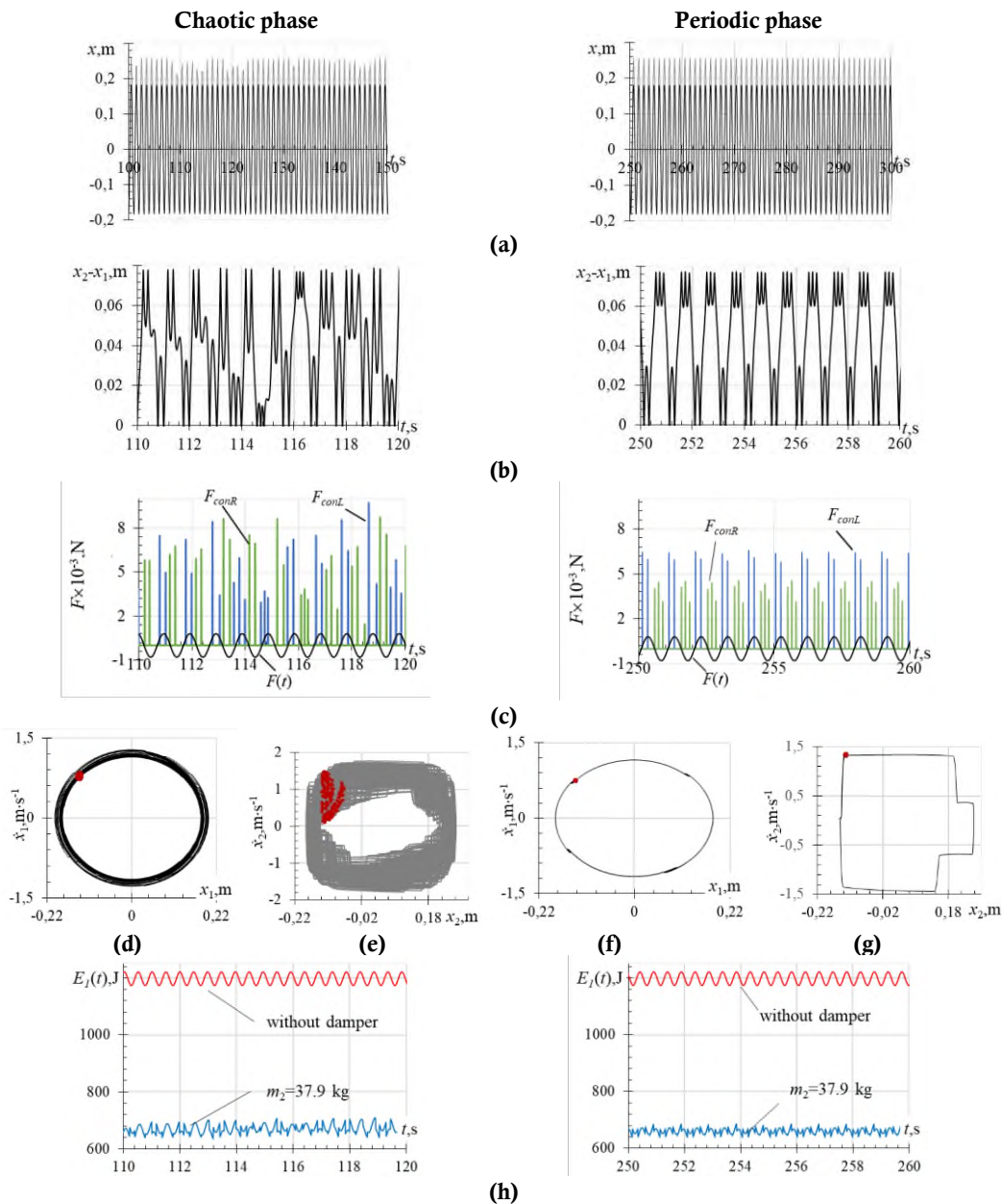


Figure 8. (Continued).

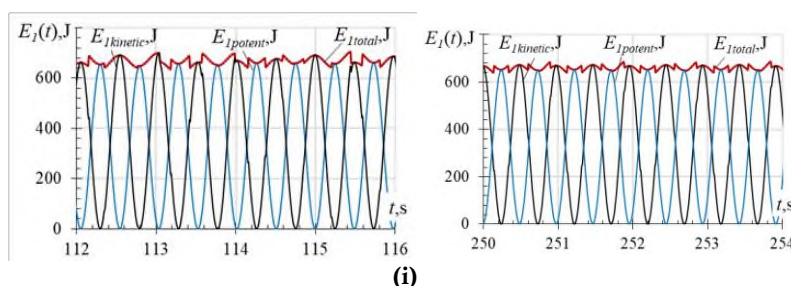


Figure 8. The movement picture of transient chaos in chaotic (left) and periodic (right) phases at $m_2 = 37.9$ kg with 7 optimized parameters at $P = 800$ N, $\omega = 6.4$ rad·s⁻¹, **(a)** the displacements of both bodies; **(b)** the relative damper displacements; **(c)** the contact forces; **(d)–(g)** the phase trajectories with Poincaré maps in red for primary structure **(d)**, **(f)** and damper **(e)**, **(g)**; **(h)**, **(i)** the primary structure energy.

5. Conclusions

The performed and described studies gave grounds for the following conclusions.

- The vibro-impact damper under consideration—SSVI NES—is quite effective in a wide range of the exciting force amplitude and in the range of its frequency, which are higher than the resonant frequency.
- The resonant peak is shifted to the left towards low frequencies when a vibro - impact damper is attached. Attenuation of the primary structure energy at the exciting force frequencies below the resonant one does not occur.
- The dynamics of a vibro-impact system, consisting of a primary structure and a coupled damper, is rich and complex. The periodic regimes of different periodicity with different damper impact number both on the primary structure and on the obstacle occur. The chaotic motion and the transient chaos with bilateral impacts are also implemented. However, the emerging complex modes do not reduce the damper efficiency, since the oscillatory amplitudes and velocities of the primary structure change little under these regimes, but the contact forces change strongly.
- Thus, the damper efficiency is quite stable in those ranges of the exciting force parameters where mitigation occurs.
- The considered single-sided VI NES actually works as a double-sided VI NES, since the damper impacts are bilateral both on the primary structure on the left and on the obstacle on the right. The primary structure in this case plays the role of the second barrier.
- Of the two options considered, the heavier damper turned out to be more effective.
- The impact contact forces are much greater than the exciting force.
- A synergistic effect is obtained by optimizing 7 damper parameters. Comparison of system responses in this case with responses of the system with 3 optimized damper parameters shows their improvement, namely a slight increase in damper efficiency and the implementation of smoother motion modes. The main improvement is the absence of bursts in the implemented motion regimes, since it is during bursts that the primary structure amplitudes increase sharply and the damper efficiency reduces.

To summarize, it is necessary to emphasize the limitations of VI NES: they do not mitigate the primary structure energy at low exciting force frequencies, lower than resonant one. In addition, it is worth noting the difficulty of its tuning, that is, choosing a damper design that should ensure its effective operation, which will become a practical problem when using it. It is believed that VI NES will be useful for mitigation of the energy of the high-rise buildings and towers under transient loading. This study as

other similar ones “facilitates the implementation of NESs in real-life structures and applications in the future.”

Author contributions

Conceptualization, PL and OP; methodology, OP; software, TP; validation, PL, OP, and TP; writing—original draft preparation, OP; writing—review and editing, OP and TP; visualization, TP; project administration, PL; funding acquisition, PL. All authors have read and agreed to the published version of the manuscript.

Conflict of interest

The authors declare no conflict of interest.

References

1. Gutierrez Soto M, Adeli H. Tuned mass dampers. *Archives of Computational Methods in Engineering* 2013; 20(4): 419–431. doi: 10.1007/s11831-013-9091-7
2. Rahimi F, Aghayari R, Samali B. Application of tuned mass dampers for structural vibration control: A state-of-the-art review. *Civil Engineering Journal* 2020; 6(8): 1622–1651. doi: 10.28991/cej-2020-03091571
3. Ding H, Chen LQ. Designs, analysis, and applications of nonlinear energy sinks. *Nonlinear Dynamics* 2020; 100(4): 3061–3107. doi: 10.1007/s11071-020-05724-1
4. Saeed AS, Abdul Nasar R, AL-Shudeifat MA. A review on nonlinear energy sinks: Designs, analysis and applications of impact and rotary types. *Nonlinear Dynamics* 2022; 111(1): 1–37. doi: 10.1007/s11071-022-08094-y
5. Vakakis AF. Passive nonlinear targeted energy transfer. *Philosophical Transactions of the Royal Society A: Mathematical, Physical and Engineering Sciences* 2018; 376(2127): 20170132. doi: 10.1098/rsta.2017.0132
6. Lu Z, Wang Z, Masri SF, Lu X. Particle impact dampers: Past, present, and future. *Structural Control and Health Monitoring* 2017; 25(1): e2058. doi: 10.1002/stc.2058
7. Ibrahim RA. Recent advances in nonlinear passive vibration isolators. *Journal of Sound and Vibration* 2018; 314(3–5): 371–452. doi: 10.1016/j.jsv.2008.01.014
8. Lee YS, Vakakis AF, Bergman LA, et al. Passive non-linear targeted energy transfer and its applications to vibration absorption: A review. *Proceedings of the Institution of Mechanical Engineers, Part K: Journal of Multi-body Dynamics* 2008; 222(2): 77–134. doi: 10.1243/14644193jmbd118
9. Wang J, Wierschem NE, Spencer BF, Lu X. Track nonlinear energy sink for rapid response reduction in building structures. *Journal of Engineering Mechanics* 2015; 141(1): 04014104. doi: 10.1061/(ASCE)EM.1943-7889.0000824
10. Wierschem NE. *Targeted Energy Transfer Using Nonlinear Energy Sinks for the Attenuation of Transient Loads on Building Structures* [PhD thesis]. University of Illinois at Urbana-Champaign; 2014.
11. Li T. *Study of Nonlinear Targeted Energy Transfer by Vibro-Impact* [PhD thesis]. National Institute of Applied Sciences of Toulouse; 2016.
12. Qui D. *Theoretical and Experimental Study of Tuned Nonlinear Energy Sink Application to Passive Vibration Control* [PhD thesis]. National Institute of Applied Sciences of Toulouse; 2018.
13. Youssef B, Leine RI. A complete set of design rules for a vibro-impact NES based on a multiple scales approximation of a nonlinear mode. *Journal of Sound and Vibration* 2021; 501: 116043. doi: 10.1016/j.jsv.2021.116043
14. Bergeot B, Bellizzi S, Berger S. Dynamic behavior analysis of a mechanical system with two unstable modes coupled to a single nonlinear energy sink. *Communications in Nonlinear Science and Numerical Simulation* 2021; 95: 105623. doi: 10.1016/j.cnsns.2020.105623
15. Saeed AS, AL-Shudeifat MA, Cantwell WJ, Vakakis AF. Two-dimensional nonlinear energy sink for effective passive seismic mitigation. *Communications in Nonlinear Science and Numerical Simulation* 2021; 99: 105787. doi: 10.1016/j.cnsns.2021.105787
16. Luo J, Wierschem NE, Hubbard SA, et al. Large-scale experimental evaluation and numerical simulation of a system of nonlinear energy sinks for seismic mitigation. *Engineering Structures* 2014; 77: 34–48. doi: 10.1016/j.engstruct.2014.07.020
17. Qiu D, Seguy S, Paredes M. Design criteria for optimally tuned vibro-impact nonlinear energy sink. *Journal of Sound and Vibration* 2019; 442: 497–513. doi: 10.1016/j.jsv.2018.11.021

18. Gourc E, Seguy S, Michon G, et al. Quenching chatter instability in turning process with a vibro-impact nonlinear energy sink. *Journal of Sound and Vibration* 2015; 355: 392–406. doi: 10.1016/j.jsv.2015.06.025
19. Wierschem NE, Hubbard SA, Luo J, et al. Response attenuation in a large-scale structure subjected to blast excitation utilizing a system of essentially nonlinear vibration absorbers. *Journal of Sound and Vibration* 2017; 389: 52–72. doi: 10.1016/j.jsv.2016.11.003
20. Javidialesaadi A, Wierschem NE. Optimal design of rotational inertial double tuned mass dampers under random excitation. *Engineering Structures* 2018; 165: 412–421. doi: 10.1016/j.engstruct.2018.03.033
21. Wu Z, Seguy S, Paredes M. Basic constraints for design optimization of cubic and bistable nonlinear energy sink. *Journal of Vibration and Acoustics* 2022; 144(2): 021003. doi: 10.1115/1.4051548
22. Li T, Seguy S, Berlioz A. Optimization mechanism of targeted energy transfer with vibro-impact energy sink under periodic and transient excitation. *Nonlinear Dynamics* 2016; 87(4): 2415–2433. doi: 10.1007/s11071-016-3200-8
23. Li W, Wierschem NE, Li X, et al. Numerical study of a symmetric single-sided vibro-impact nonlinear energy sink for rapid response reduction of a cantilever beam. *Nonlinear Dynamics* 2020; 100(2): 951–971. doi: 10.1007/s11071-020-05571-0
24. AL-Shudeifat MA, Saeed AS. Comparison of a modified vibro-impact nonlinear energy sink with other kinds of NESs. *Meccanica* 2020; 56(4): 735–752. doi: 10.1007/s11012-020-01193-3
25. Farid M. Dynamics of a hybrid cubic vibro-impact oscillator and nonlinear energy sink. *Communications in Nonlinear Science and Numerical Simulation* 2023; 117: 106978. doi: 10.1016/j.cnsns.2022.106978
26. Feudo SL, Job S, Cavallo M, et al. Finite contact duration modeling of a vibro-impact nonlinear energy sink to protect a civil engineering frame structure against seismic events. *Engineering Structures* 2022; 259: 114137. doi: 10.1016/j.engstruct.2022.114137
27. Theurich T, Krack M. Experimental validation of impact energy scattering as concept for mitigating resonant vibrations. *Journal of Structural Dynamics* 2023; (2): 1–23. doi: 10.25518/2684-6500.126
28. Bazhenov VA, Pogorelova OS, Postnikova TG. Comparison of two impact simulation methods used for nonlinear vibro-impact systems with rigid and soft impacts. *Journal of Nonlinear Dynamics* 2013; 2013: 1–12. doi: 10.1155/2013/485676
29. Bazhenov V, Pogorelova O, Postnikova T. Crisis-induced intermittency and other nonlinear dynamics phenomena in vibro-impact system with soft impact. In: Altenbach H, Amabili M, Mikhlin YV (editors). *Nonlinear Mechanics of Complex Structures: From Theory to Engineering Applications*. Springer; 2021. pp.185–203.
30. Foale S, Bishop SR. Bifurcations in impact oscillations. *Nonlinear Dynamics* 1994; 6(3): 285–299. doi: 10.1007/BF00053387
31. Johnson KL. *Contact Mechanics*. Cambridge University Press; 1985.
32. Costa D, Kuske R, Yurchenko D. Qualitative changes in bifurcation structure for soft vs hard impact models of a vibro-impact energy harvester. *Chaos: An Interdisciplinary Journal of Nonlinear Science* 2022; 32(10): 103120. doi: 10.1063/5.0101050
33. Lizunov P, Pogorelova O, Postnikova T. Choice of the model for vibro-impact nonlinear energy sink. *Strength of Materials and Theory of Structures* 2022; (108): 63–76. doi: 10.32347/2410-2547.2022.108.63-76
34. Lizunov P, Pogorelova O, Postnikova T. Dynamics of primary structure coupled with single sided vibro-impact nonlinear energy sink. *Strength of Materials and Theory of Structures* 2022; (109): 103–113. doi: 10.32347/2410-2547.2022.109.20-29
35. Lizunov P, Pogorelova O, Postnikova T. Vibro-impact damper dynamics depending on system parameters. *Research Square* 2023. 1–20. doi: 10.21203/rs.3.rs-2786639/v1
36. Bazhenov VA, Pogorelova OS, Postnikova TG. Transient chaos in platform-vibrator with shock. *Strength of Materials and Theory of Structures* 2021; (106): 103–123. doi: 10.32347/2410-2547.2021.106.22-40
37. Szaksz B, Stepan G. Transient chaotic behavior of fuzzy controlled polishing processes. *Chaos: An Interdisciplinary Journal of Nonlinear Science* 2022; 32(9): 093112. doi: 10.1063/5.0101257
38. Lamarque CH, Janin O. Modal analysis of mechanical systems with impact non-linearities: Limitations to a modal superposition. *Journal of Sound and Vibration* 2000; 235(4): 567–609. doi: 10.1006/jsvi.1999.2932